Clustering phenomena in nuclear matter below the saturation density

Hiroki Takemoto,[1,2] Masahiro Fukushima,[1] Satoshi Chiba,[1] Hisashi Horiuchi,[3] Yoshinori Akaishi,[4] and Akihiro Tohsaki[2]
[1]*Advanced Science Research Center, Japan Atomic Energy Research Institute, Tokai, Ibaraki 319-1195, Japan*
[2]*Department of Fine Materials Engineering, Shinshu University, Ueda 386-8567, Japan*
[3]*Department of Physics, Kyoto University, Kyoto 606-8502, Japan*
[4]*Institute of Particle and Nuclear Studies, KEK 305-0801, Japan*
(Received 2 December 2003; published 16 March 2004)

We investigate density-fluctuated states of nuclear matter as a result of clustering below the saturation density ρ_0 by description in terms of the Bloch function. The Bloch description has the advantage of a unified representation for a density-fluctuated state from an aggregate of uncorrelated clusters in extremely low-density regions to the plane-wave state of uniform matter in relatively high-density regions. We treat the density-fluctuated states due to α and ^{16}O clustering in symmetric nuclear matter and due to ^{10}He clustering in asymmetric nuclear matter. The density-fluctuated states develop as the density of matter decreases below each critical density around $0.2-0.4\ \rho_0$ which depends on what kind of effective force we use.

DOI: 10.1103/PhysRevC.69.035802 PACS number(s): 21.65.+f, 26.60.+c, 21.60.Gx

I. INTRODUCTION

In many cases, nucleons in a nucleus are considered as independent particles moving in an average potential created by all the nucleons. On the basis of this idea, the ground state of nuclear matter is considered to be uniform near the nuclear saturation density such as in the interior region of nuclei. Therefore, the ground state of infinite nuclear matter is described by the Slater determinant wave function of plane-wave single-particle states. Overhauser [1] was the first to consider the stability of the plane-wave solution of nuclear matter. He found that if one assumes the existence of density-fluctuated states (DFSs) instead of plane-wave states, there could be a considerable gain in the binding energy.

If uniform nuclear matter is unstable and prefers to form clusters below the saturation density, it is expected from the importance of α-clustering effects in light nuclei [2] that this might be due to some periodic distribution of α clusters similar to the structures of ideal crystals. Akaishi and Bandō investigated a periodic DFS due to α clustering by using the Bloch function in analogy with electrons in crystals [3]. Brink and Castro [4], and Tohsaki [5,6] also studied the existence of a lattice structure of α clusters by the generator coordinate method. Their results suggest that α-clustering effects might be important in low-density regions such as the surface region of heavy nuclei. Furthermore, recent theoretical investigations suggest the possibility of α-particle condensation in low-density nuclear matter [7,8]. Although the above studies have led to some understanding of the α-clustering effect in symmetric nuclear matter, nothing has been said about DFSs due to clustering in asymmetric nuclear matter and about DFSs due to the clustering of clusters heavier than α clusters.

In extremely low-density regions like the inner crust of neutron stars, crystalline structure of ^{56}Fe is expected because ^{56}Fe is the nucleus with the most binging energy per nucleon. At subsaturation densities, liquid drop models proposed several characteristic geometrical structures of dilute nuclear matter, such as spherical, rodlike, and slablike nuclei [9,10]. Inhomogeneous states of nuclear matter at subsaturation densities are also studied by a quantum molecular-dynamics (QMD) model, which is a rather quasiclassical molecular-dynamics model [11–13]. Especially, Watanabe *et al.* reproduced the geometrical structure of dilute nuclear matter proposed by liquid drop models by treating the long-range property of the Coulomb interaction [13]. QMD simulations provided an insight into the properties of nonuniform dilute nuclear matter in a microscopic point of view.

However, in the QMD method, the fermionic nature of nucleons, the Fermi motion, and the exchange effects are simulated by an effective potential. It is highly desirable to represent DFSs by the antisymmetrized wave function. Pozamantir and Overhauser investigated a one-dimensional DFS of symmetric nuclear matter in the quantum treatment using the Bloch function [14]. They found that the binding energy of the system increases compared with that for uniform nuclear matter due to density fluctuation with a $15-27$ fm wavelength, which corresponds to the slablike nuclei in liquid drop models.

The aim of our study is to understand the clustering properties of nuclear matter as the many-body quantum system. As the first step, we treat here the DFS with the simple cubic periodicity due to ^{16}O clustering as well as α-clustering in symmetric nuclear matter and due to ^{10}He clustering in asymmetric nuclear matter. We describe DFSs due to clustering by a Slater determinant wave function where single-particle states of nucleons are represented by the Bloch function. For the purpose of treating DFSs due to the clustering up to $0p$-shell nuclei, we extended the Bloch description in Ref. [3] using the tight-binding approximation to include the $0s$ and $0p$ orbits. The Bloch description has the advantage of a unified representation for DFS from an aggregate of uncorrelated clusters in extremely low-density regions to the plane-wave state of uniform matter in relatively high-density regions. Section II explains the Bloch description. Section III investigates energy behaviors of DFSs due to clustering of doubly closed-shell nuclei ^{4}He, ^{16}O, and ^{10}He. Section III A shows the general energy profile of DFSs, and, in Sec III B, we attempt to estimate the spurious energy of each constituent cluster, which originates in its center-of-mass motion.

Section III C describes the transition from the simple cubic lattice of ^{16}O to the face-centered-cubic lattice of α particles with the density of matter within the classical treatment. Section III D shows that critical densities at which DFSs start to develop depends on what kind of effective force we use. Finally, Sec. IV includes the summary and discussion.

II. DESCRIPTION OF A DENSITY-FLUCTUATED STATE WITH PERIODICITY

We consider a DFS as a simple cubic lattice of nuclei with mass number A. The lattice is considered to be built from N^3 cubic unit cells with side a. We consider a variational total wave function of a system in analogy with electrons in a lattice as follows:

$$\Phi = \mathcal{A}\prod_{i=1}^{AN^3} \psi_{o_i \boldsymbol{k}_i}(\boldsymbol{r}_i)\cdot\chi_i(\sigma_i,\tau_i), \tag{1}$$

where $\psi_{o_i \boldsymbol{k}_i}$ and χ_i represent the spatial and spin-isospin parts of the ith single-particle wave function of nucleons, respectively. The nucleons are assumed to occupy Bloch functions constructed from atomic orbits under the periodic boundary condition. The subscripts o_i and $\boldsymbol{k}_i$ denote an atomic orbital and a Bloch wave number vector, $\boldsymbol{k}_i=(2\pi/Na)\boldsymbol{n}_i$ with $\boldsymbol{n}_i$ being an integer vector (n_{ix},n_{iy},n_{iz}). The Bloch wave number vectors $\{\boldsymbol{k}_i\}$ become continuous variables $\boldsymbol{k}$ as N approaches infinity.

In Ref. [3] the DFS due to α clustering was described by using the 0s orbital Bloch function as follows:

$$\psi_{s\boldsymbol{k}}(\boldsymbol{r}) = \phi_{sk_x}(x)\cdot\phi_{sk_y}(y)\cdot\phi_{sk_z}(z), \tag{2}$$

$$\phi_{sk}(x) = \frac{1}{\mathcal{N}_{sk}^{1/2}}\left(\frac{1}{N}\right)^{1/2}\sum_{m=-N/2}^{N/2} e^{ikma}\varphi_s(x-ma), \tag{3}$$

and

$$\varphi_s(x) = \left(\frac{2}{\pi b^2}\right)^{1/4} e^{-x^2/b^2}, \tag{4}$$

where m is an integer, and $\mathcal{N}_{sk}$ is a normalization factor. The 0s orbital Bloch functions $\{\phi_{sk}\}$ are orthonormal functions, $\langle\phi_{sk}|\phi_{sk'}\rangle=\delta_{kk'}$.

For DFSs due to clustering of 0p-shell nuclei, we assume that nucleons occupy 0p orbital Bloch states in addition to the 0s orbital ones. The 0p orbital Bloch function orthogonal to the 0s orbital one (2) are defined as follows:

$$\psi_{op_x\boldsymbol{k}}(\boldsymbol{r}) = \phi_{opk_x}(x)\cdot\phi_{sk_y}(y)\cdot\phi_{sk_z}(z), \tag{5a}$$

$$\psi_{op_y\boldsymbol{k}}(\boldsymbol{r}) = \phi_{sk_x}(x)\cdot\phi_{opk_y}(y)\cdot\phi_{sk_z}(z), \tag{5b}$$

$$\psi_{op_z\boldsymbol{k}}(\boldsymbol{r}) = \phi_{sk_x}(x)\cdot\phi_{sk_y}(y)\cdot\phi_{opk_z}(z), \tag{5c}$$

where

$$\phi_{opk}(x) = \frac{1}{\mathcal{N}_{opk}^{1/2}}[\phi_{pk}(x)-\langle\phi_{sk}|\phi_{pk}\rangle\phi_{sk}(x)], \tag{6}$$

$$\phi_{pk}(x) = \frac{1}{\mathcal{N}_{pk}^{1/2}}\left(\frac{1}{N}\right)^{1/2}\sum_{m=-N/2}^{N/2} e^{ikma}\varphi_p(x-ma), \tag{7}$$

$$\varphi_p(x) = \left(\frac{2}{\pi b^2}\right)^{1/4}\frac{2}{b}xe^{-x^2/b^2}, \tag{8}$$

and $\mathcal{N}_{opk}$ and $\mathcal{N}_{pk}$ are normalization factors. It is noted that the 0p orbital Bloch functions (5a)–(5c) are orthogonal not only to the 0s Bloch function (2) but also among themselves. Accordingly, the Bloch functions $\{\psi_{n\boldsymbol{k}}\}$ are orthonormal functions,

$$\langle\psi_{o\boldsymbol{k}}|\psi_{o'\boldsymbol{k}'}\rangle = \delta_{oo'}\delta_{\boldsymbol{k}\boldsymbol{k}'}, \tag{9}$$

where o and o' denote s, op_x, op_y, and op_z.

There are two parameters in the Bloch description: one is the lattice spacing a, which corresponds to the density of matter, and the other is the width parameter of harmonic oscillator wave functions b, which corresponds to the size of a cluster. The size parameter b is optimized by minimizing the expectation value of Hamiltonian at the fixed lattice parameter a. In this paper the Fermi surface is fixed to the Fermi cube $(-k_F\leqslant k_{x,y,z}\leqslant k_F, k_F=\pi/a)$.

Before proceeding to the main subject, we show the behaviors of the Bloch functions with respect to a/b. Figure 1 displays the real (left panels) and imaginary (right panels) parts of the s-wave (upper panels), p-wave (middle panels), and op-wave (lower panels) Bloch functions in the case of $a=1$ and $k=\pi/2$. At a large a/b value (the dotted line for $a/b=10$), s-wave and p-wave Bloch functions become localized single-particle wave functions at lattice sites, and the op-wave Bloch function is almost identical to the p-wave Bloch function. As the ratio a/b approaches zero, the s-wave and p-wave Bloch functions, Eqs. (3) and (7), become plane-wave functions,

$$\lim_{a/b\to 0}\phi_{sk}(x) = \frac{1}{\sqrt{L}}e^{ikx},$$

$$\lim_{a/b\to 0}\phi_{pk}(x) = \frac{1}{\sqrt{L}}e^{-i\cdot\mathrm{sgn}(k)\cdot\pi/2}e^{ikx},$$

where $L=Na$. The limit of the p-wave function shifts from the ordinary plane-wave function by the phase $-i\cdot\mathrm{sgn}(k)\cdot\pi/2$. Due to the orthogonality to the s-wave Bloch function, the op-wave Bloch function (6) becomes a plane-wave function with the wave number vector $k-\mathrm{sgn}(k)\cdot 2k_F$ in the limit that $a/b\to 0$,

$$\lim_{a/b\to 0}\phi_{opk}(x) = \frac{1}{\sqrt{L}}e^{i\cdot\mathrm{sgn}(k)\cdot\pi/2}e^{i\cdot\{k-\mathrm{sgn}(k)\cdot 2k_F\}x}.$$

Figure 2 displays the kinetic energies of the s-wave (solid lines) and op-wave (dotted lines) Bloch functions. At large a/b values (the top panel indicates the case that $a/b=5$), the kinetic energies of the s-wave and op-wave Bloch functions with any wave number vector are $(\hbar^2/2M)(1/b^2)$ and $(\hbar^2/2M)(3/b^2)$, respectively, which correspond to the kinetic energies of harmonic oscillator wave functions with quantum

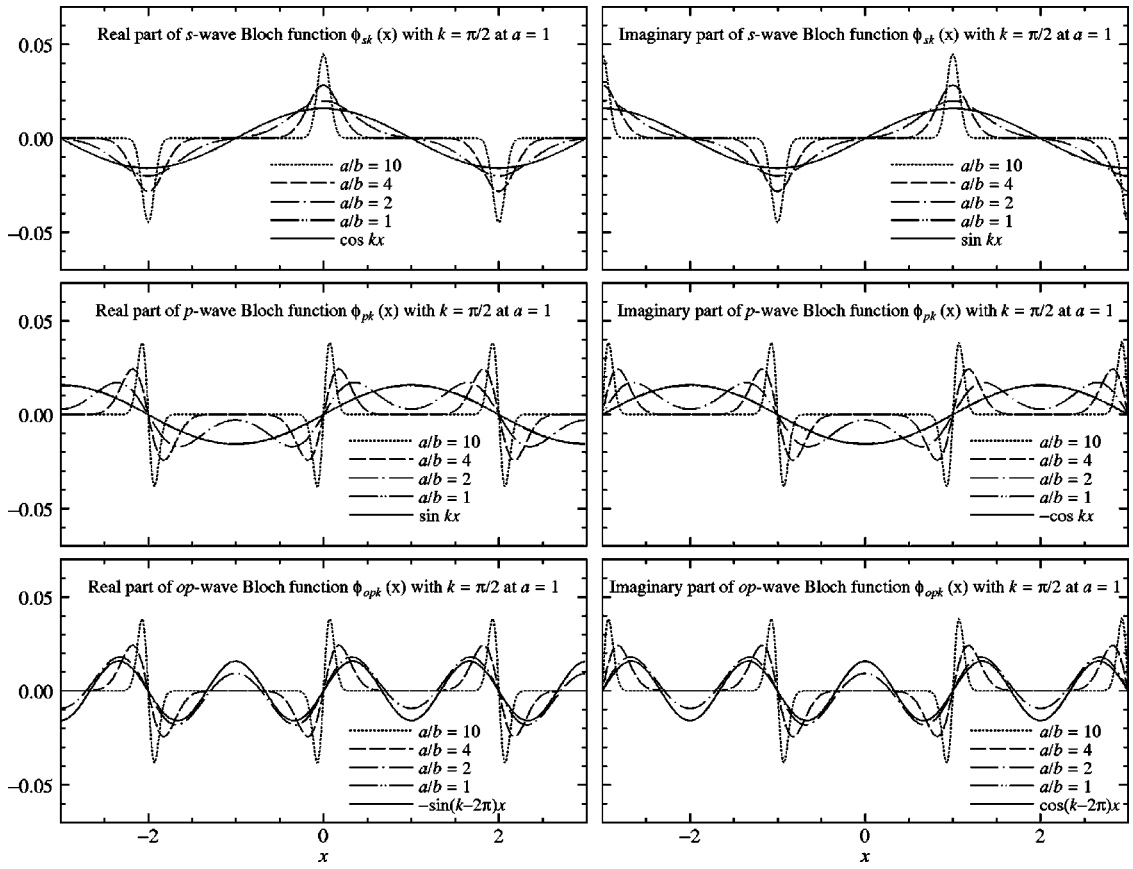

FIG. 1. Behaviors of the Bloch functions with respect to a/b in the case where $a=1$ and $k=\pi/2$. The left and right panels display real and imaginary parts of the *s*-wave (top panels), *p*-wave (middle panels), and *op*-wave (bottom panels) Bloch functions, respectively. The dotted, dashed, dotted-sashed, and two-dotted-dashed curves indicate the cases where $a/b=10,4,2$, and 1.

numbers 0 and 1, respectively. As the value of a/b decreases (from the top panel to the bottom panel), the kinetic energies of the *s*-wave and *op*-wave Bloch functions with the wave number vector k gradually approach those of plane wave: $(\hbar^2/2M)k^2$ and $(\hbar^2/2M)\{k-\mathrm{sgn}(k)\cdot 2k_F\}^2$, respectively.

Accordingly, in the limit that $a/b\rightarrow 0$, the DFS due to α-clustering described by the *s*-wave Bloch function with the Fermi cube goes to uniform matter described by the plane wave with the Fermi cube: $-k_F\leqslant k_{x,y,z}\leqslant k_F$, while the DFS due to ^{16}O clustering described by the *s*-wave and the *op*-wave Bloch functions with the Fermi cube becomes uniform matter described by the plane wave with the protruding Fermi surface,

$$\begin{aligned} &-2k_F\leqslant k_x\leqslant 2k_F, \quad -k_F\leqslant k_{y,z}\leqslant k_F,\\ &-2k_F\leqslant k_y\leqslant 2k_F, \quad -k_F\leqslant k_{z,x}\leqslant k_F,\\ &-2k_F\leqslant k_z\leqslant 2k_F, \quad -k_F\leqslant k_{x,y}\leqslant k_F. \end{aligned} \tag{10}$$

III. ENERGY BEHAVIOR OF DENSITY-FLUCTUATED STATES DUE TO CLUSTERING

First, we show the energy profiles of constituent clusters, ^{4}He, ^{16}O, and ^{10}He nuclei. The total energy per nucleon of the system is divided into four parts:

$$E = T + U_{\mathrm{nucl}} + U_{\mathrm{Coul}} - T_{\mathrm{c.m.}}. \tag{11}$$

The first term represents the kinetic energy, and the second and third terms represent the nuclear and Coulomb parts of the interaction energy, respectively. The fourth term represents the spurious energy arising from the center-of-mass (c.m.) motion of a constituent cluster. We adopt the modified Volkov force (MV1 case 3) [15], as an effective nuclear force. The MV1 force consists of the two-range Gaussian-type two-body part and the δ-type three-body part. The three-body part is indispensable to reproduce the saturation property of uniform nuclear matter. The parameters in the MV1 force are determined in order to reproduce the binding energies of doubly closed ^{4}He, ^{16}O, and ^{40}Ca nuclei. Table I lists the calculated energies per nucleon of ^{4}He, ^{16}O, and ^{10}He nuclei by using the simplest harmonic oscillator wave functions, which are compared with the experimental data. The calculated value of the saturation energy of uniform symmetric matter with the Fermi sphere is 23.51 MeV at 0.261 fm^{-3}, while the empirical value is 15.6 MeV at 0.17 fm^{-3}.

When we attempt to evaluate the expectation value of Hamiltonian (11) for DFSs, we face two problems. The first one deals with the spurious energy from the c.m. motion of each constituent cluster. It is not possible to obtain the exact value of the spurious energy for a correlated cluster in an

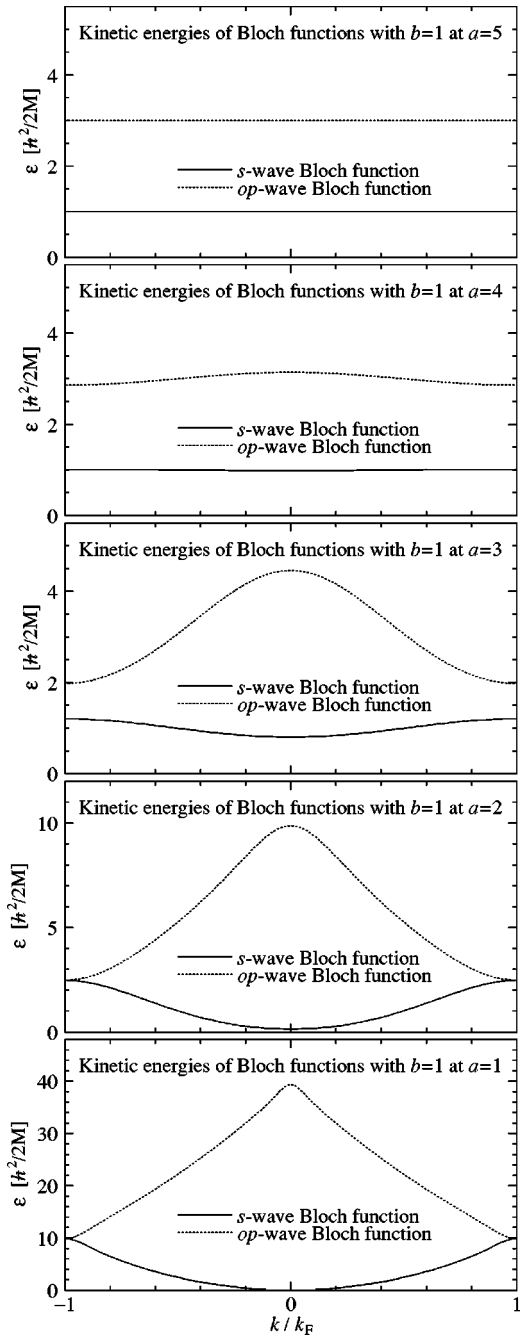

FIG. 2. Kinetic energies of the *s*-wave (solid line) and *op*-wave (dotted line) Bloch functions with $b=1$. The cases of $a=5,4,3,2,$ and 1 are displayed from top to bottom.

aggregate though it definitely can be evaluated for an isolated nucleus (cluster). The second one deals with the Coulomb energy of an infinite nuclear system. The Coulomb energy of nuclear matter diverges logarithmically unless a neutralizing background of electrons is considered. In uniform nuclear matter, the Coulomb energy becomes zero due to complete cancellation of positive and negative charge distributions. However, if a DFS arises, the Coulomb energy obtains a certain value due to the difference between positive and negative charge distributions [16].

Section III A describes the energy behaviors of DFSs as a function of the average density, ignoring the spurious and Coulomb energies. In Table I, the energy values obtained by excluding the Coulomb energy and/or spurious energies have also been listed. Especially, an α cluster has considerable spurious energy coming from the zero-point oscillation in its c.m. motion, as indicated in Table I. We estimate this in terms of the single-particle kinetic energy of the 0*s* orbital Bloch state with $\boldsymbol{k}=0$ in Sec. III B. In Sec. III C, the crystalline structure of α particles in the uniform background of electrons has been discussed within the classical treatment. Finally, the dependence of energy behaviors of DFSs on effective forces has been analyzed in Sec. III D.

A. Development of density fluctuation due to clustering with the decrease of density

We first show that the energies of DFSs described by the Bloch function smoothly change from an aggregate of isolated clusters fixed at lattice sites to uniform matter (plane-wave states) with the increase of density. Figure 3 shows the energy curves of the DFS due to ^{4}He (left panel) and ^{16}O (right panel) clustering as a function of the width parameter b at the fixed lattice spacing a. Here, the Coulomb and spurious energies are ignored. In the region of the small width parameters, energy curves at various fixed lattice sides a are almost similar to those of the isolated cluster limit (solid lines). As the width parameter b increases, the energy curves deviate from the isolated cluster limit and approach the expectation value of plane-wave states (uniform matter), which are indicated by the arrows on the right. The deviation from the isolated cluster limit increases with a decrease in lattice spacing a (density increasing).

It should be noted that the energy curve has a minimum point (crosses), and its energy is lower than that of the plane-wave state. This means that the DFS is energetically favorable compared to the plane-wave state. This minimum point shifts to the larger width parameter when the lattice spacing a decreases. In other words, the density fluctuation gradually decreases as the density of matter increases, and an aggregate of clusters finally melts into uniform matter.

Figure 4 summarizes the minimum energy points of DFSs shown in Fig. 3. The left panel displays energy curves of DFSs due to ^{4}He (two-dotted-dashed line) and ^{16}O (dotted-dashed line) clustering in symmetric nuclear matter as a function of the density of matter. The right panel depicts the case of ^{10}He (dotted line) clustering in asymmetric nuclear matter with the proton ratio $Y_p=0.2$. In the left panel, the dashed curve indicates the uniform limit of the DFS due to ^{4}He clustering, and the solid curve indicates the uniform limit of the DFS due to ^{16}O clustering. The solid curve in the right panel indicates the uniform limit of the DFS due to ^{10}He clustering. It should be noted that the energy of the uniform limit of the DFS due to ^{16}O clustering is slightly lower than that due to ^{4}He clustering. Such a difference is caused by the difference between the Fermi surfaces of the two uniform limits, namely, the uniform limit of the DFS due to ^{4}He clustering has the cubic Fermi surface, while that due to ^{16}O clustering has the protruding Fermi surface given by Eq. (10). In both panels, arrows on the left indicate the energies of isolated clusters (nuclei), ignoring the Coulomb and spurious energies listed in Table I.

TABLE I. Binding energies per nucleon of ^{4}He, ^{16}O, and ^{10}He nuclei using MV1 force and the wave functions of the simplest harmonic oscillator shell model. In each nucleus, the first row represents the minimized total energy, the second represents the minimized energy excluding U_{Coul}, and the third one represents the minimized energy excluding U_{Coul} and $T_{\mathrm{c.m.}}$.

	b(fm)	T(MeV)	U_{nucl}(MeV)	U_{Coul}(MeV)	$T_{\mathrm{c.m.}}$(MeV)	Theor. E(MeV)	Expt. E(MeV)
^{4}He	2.14	13.58	−17.57	0.19	3.40	−7.19	−7.07
	2.14	13.58	−17.57		3.40	−7.38	
	2.31	11.66	−15.88			−4.22	
^{16}O	2.45	15.54	−23.65	0.86	0.65	−7.90	−7.98
	2.44	15.67	−23.90		0.65	−8.76	
	2.46	15.43	−23.53			−8.11	
^{10}He	2.59	12.98	−14.80	0.06	0.93	−2.68	−3.02
	2.59	12.98	−14.80		0.93	−2.74	
	2.70	11.95	−13.80			−1.85	

As clearly seen, we are able to recognize that the Bloch description smoothly describes the disappearance of density fluctuation with the density of matter from an aggregate of isolated clusters to uniform matter. Furthermore, we immediately find that the DFS due to ^{16}O clustering is always energetically favorable as compared with that due to ^{4}He clustering. However, we must not arrive at a conclusion hastily because the spurious and Coulomb energies are ignored in the present calculations. Especially, as was shown in Table I, a ^{4}He cluster has considerable spurious energy. In the following section, we attempt to remove the spurious energy of each constituent cluster correlating among them.

B. Spurious energy of the c.m. motion of each constituent cluster with correlation

The energies of DFSs shown in Fig. 4 include the spurious energy originating from the c.m. motion of each constituent cluster. In extremely low-density regions (very large values of the ratio a/b), clusters placed at different lattice sites does not correlate; therefore, we should subtract the zero-point oscillation energy from the energy of DFSs in the c.m. motion of each cluster,

$$T_0 = \frac{3\hbar^2}{2M\,A}\frac{1}{b^2}, \tag{12}$$

where M is the mass of a nucleon and A is the mass number of the cluster. In relatively high-density regions (very small values of the ratio a/b), constituent clusters melt into uniform matter and in principle, the spurious energy becomes zero. In intermediate-density regions, it is not possible to evaluate the spurious energy precisely, but it must satisfy the following condition:

$$0 \leqq T_{\mathrm{c.m.}} \leqq T_0. \tag{13}$$

Tohsaki evaluated the spurious energy for α-cluster matter by solving the dynamical equation where one of the α clusters is allowed to move in its cavity formed by all the other α clusters at lattice sites in the framework of the generator coordinate method [6].

Here, we estimate the spurious energy from the feature of the kinetic energy of the 0s orbital Bloch function with $k=0$. As shown in Fig. 2, the kinetic energy of the 0s orbital Bloch function with $k=0$ changes from AT_0 to 0 as the ratio a/b decreases. We first define the development of the cluster,

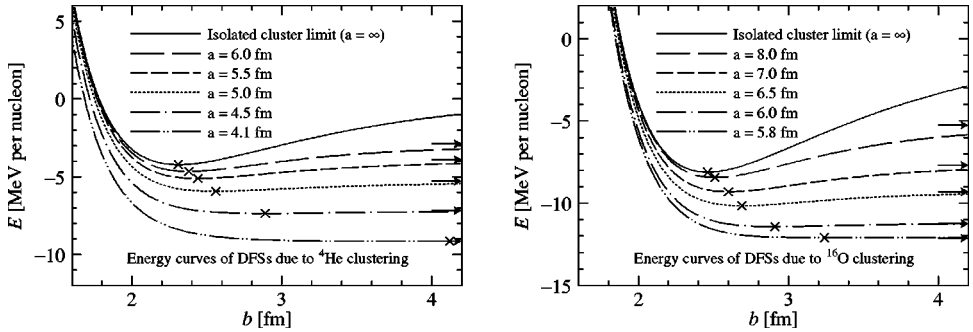

FIG. 3. Energy curves of DFSs due to ^{4}He (left panel) and ^{16}O (right panel) clustering as a function of the width parameter b at various fixed lattice spacing a. In the left panel, the long-dashed, short-dashed dotted, dotted-dashed, and two-dotted-dashed curves show energy curves at $a=6.0, 5.5, 5.0, 4.5$, and 4.1 fm, respectively. In the right panel, the long-dashed, short-dashed dotted, dotted-dashed, and two-dotted-dashed curves show energy curves at $a=8.0, 7.0, 6.5, 6.0$, and 5.8 fm, respectively. The solid curve shows the energy curve of the isolated cluster limit ($a=\infty$) in each panel. The arrows on the right denote the energies of plane-wave states (uniform matter). The crosses display the minimum energy points of DFSs at each lattice spacing a.

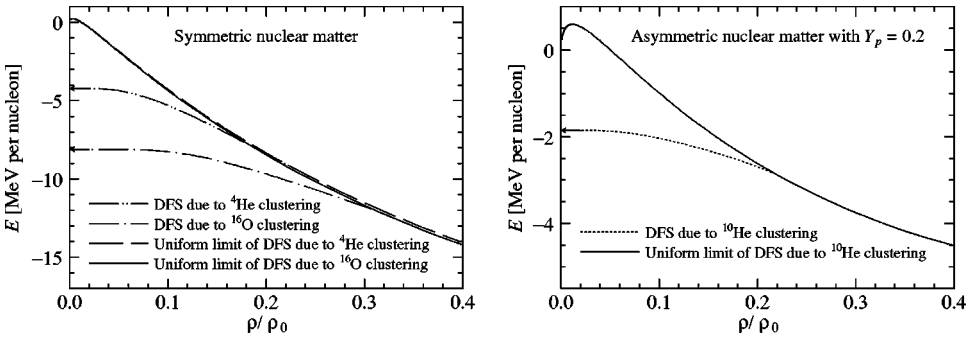

FIG. 4. Energy curves of DFSs in the symmetric (left panel) and asymmetric nuclear matter with the proton ration $Y_p=0.2$ (right panel) as a function of the density of matter. The density is normalized by the theoretical saturation density of the symmetric matter with the Fermi sphere, $\rho_0=0.261$ fm^{-3}, using the Modified Volkov force. The two-dotted-dashed, dotted-dashed, and dotted curves show the density dependence of the energies of DFSs due to ^{4}He ^{16}O, and ^{10}He clustering ignoring the Coulomb and spurious energies, respectively. In the left panel, the dashed curve indicates the plane-wave state with the Fermi surface of the proton and neutron cubes (the uniform limit of the DFS due to ^{4}He clustering), and the solid curve indicates the plane-wave state with the Fermi surface of proton and neutron Eq. (10) (the uniform limit of the DFS due to ^{10}He clustering). The arrows on the left in each panel indicate the energies of isolated clusters (nuclei) ignoring the Coulomb and spurious energies listed in Table I.

N_c, as the ratio of the kinetic energy of the 0*s* orbital Bloch function (3) to that of the 0*s* harmonic oscillator wave function (4),

$$N_c = \langle \phi_{s0}|\hat{t}_x|\phi_{s0}\rangle / \langle \varphi_s|\hat{t}_x|\varphi_s\rangle. \tag{14}$$

Figure 5 displays the behavior of N_c with respect to a/b. It changes from unity at the isolated cluster limit ($a/b\to\infty$) to zero at the uniform limit ($a/b\to 0$). Accordingly, it is reasonable to assume that N_c is regarded as the development of cluster. We estimate the spurious energy of each constituent cluster correlating among them on the basis of the development of cluster N_c as follows:

$$T_{\text{c.m.}} = T_0 N_c. \tag{15}$$

It fulfills the inequality (13).

We reoptimize the width parameter b to minimize the expectation value of Hamiltonian from which the spurious energy of each constituent cluster is subtracted according to Eq. (15). Figure 6 shows the dependence of energies of the DFSs due to ^{4}He, ^{16}O, and ^{10}He clustering on the density of matter. In the zero-density limit, the energy per nucleon of each DFS becomes the corresponding energy of the isolated cluster without the Coulomb energy (arrows at the left), which are given in Table I. After subtracting the spurious energy, the energy of each DFS also approaches that of the corresponding uniform limit with the increase of density.

Compared with the results in Fig. 4 before subtracting the spurious energy, the energy difference between DFSs due to ^{4}He and ^{16}O clustering becomes small, but there is no inversion between them. Furthermore, critical densities are not affected by whether or not the spurious energy is subtracted. This is because the single-particle state represented by the Bloch function is almost identical to the plane-wave state near critical densities and DFSs scarcely possess any spurious energy. The critical densities of the DFSs due to ^{4}He, ^{16}O, and ^{10}He clustering are listed in Table II. Here, we define the critical density from the DFS to the uniform state, as the density in which the optimized width parameter b is equal to the lattice spacing a where the development of cluster N_c is zero.

In a similar manner, the Coulomb energy may not affect the critical densities of the DFSs. We usually assume that a uniform background of electrons neutralizes nuclear matter. Near critical densities DFSs are almost uniform; therefore, the Coulomb energy is expected to be zero because of the complete cancellation between positive and negative charge distributions. Accordingly, in a uniform background of electrons, the Coulomb energy causes no inversion between energies of DFSs due to ^{4}He and ^{16}O clustering. Below critical densities, the difference becomes small because the internal Coulomb energy of a constituent cluster raises the energy of the DFS due to ^{16}O clustering compared with that due to ^{4}He clustering.

Before concluding that the DFS due to ^{16}O clustering is always energetically favorable compared with the DFS due to ^{4}He clustering, we must inspect the lattice structure of clusters because so far we have only considered DFSs with the simple cubic lattice (SCL) of clusters. In the following section, we investigate the transition of the lattice structure of α particles within the classical treatment and point out the possibility that the ^{16}O cluster is further divided into α clusters near a critical density in the nuclear matter medium.

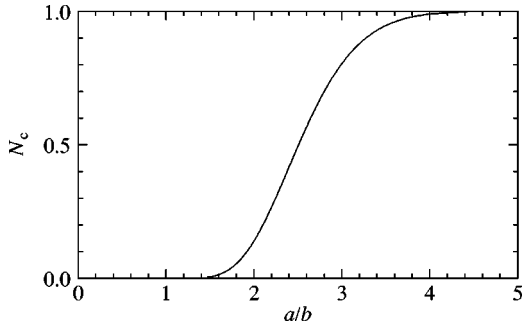

FIG. 5. Behavior of the development of cluster N_c defined by Eq. (14) with respect to a/b.

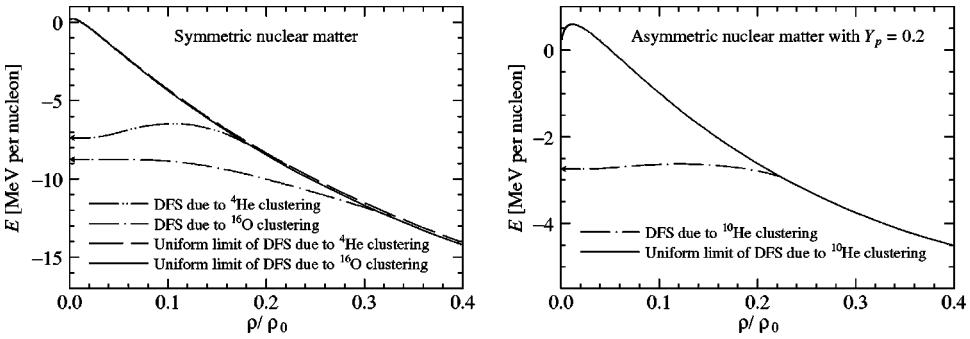

FIG. 6. Energy curves of DFSs due to ^{4}He and ^{16}O clustering in the symmetric nuclear matter (the left panel) and ^{10}He clustering in the asymmetric nuclear matter with $Y_p=0.2$ (the right panel), which are calculated by taking into account the correction of the spurious c.m. energies of individual clusters. The presentation of the curves in similar to that in Fig. 4.

C. Transition of lattice structure of α particles

We regard an α cluster as a classical point charge with $2e$ and consider an aggregate of α particles in a uniform background of electrons. As an effective α-α potential, we adopt the Lennard-Jones $(6,12)$ potential,

$$u_{\alpha-\alpha}=u_0\{(r_0/r)^{12}-2(r_0/r)^6\},$$

where r is the interparticle distance, u_0 is the depth of the potential well ($u_0>0$), and r_0 is the pair bonding length. The parameters u_0 and r_0 are set as $u_0=4.14$ MeV and $r_0=3.30$ fm to reproduce the binding energy of the ^{16}O nucleus and the saturation property of nuclear matter. The binding energy of ^{16}O that has a regular tetrahedron of α particles whose sides are 3.32 fm is 14.40 MeV below the threshold of 4α decay, which is coincident with the experimental data.

The Coulomb and Lennard-Jones potential energies of an aggregate of point charges are evaluated by the expressions derived in Ref. [16]. In a classical description like QMD in which the width of Gaussians is fixed, uniformity implies the uniform distribution of point particles. If we recognize the face-centered-cubic lattice (FCCL), which is the close-packed lattice, of α particles as the uniform nuclear matter, the saturation energy is -16.0 MeV at 0.172 fm^{-3} taking into account the internal energy of an α particle (-28.3 MeV).

We describe the transition between the SCL of ^{16}O clusters and the FCCL of α particles in the following manner. The FCCL consists of four SCLs. When the relative distances among the SCLs of α particles is small, it can be regarded as the SCL of ^{16}O with a regular tetrahedron of α particles. On the other hand, when four SCLs are at the center of face of one another, it is regarded as the FCCL of α particles. Figure 7 shows the density dependence of energies per nucleon of the SCL (dashed curve) and the FCCL (solid curve) of α particles, and the SCL of ^{16}O (dotted curve). As clearly evident, the SCL of ^{16}O is the most stable among the three lattice structures in the low-density region. As the density of matter increases, the sides of a regular tetragonal also increase, and the SCL of ^{16}O changes to the FCCL of α particles. Accordingly, it remains a possibility that the transition of the lattice structure may occur between the SCL of ^{16}O cluster and the FCCL of ^{4}He cluster, especially, near the critical density.

Furthermore, considering the uniform limit of the Bloch description, it is necessary to discuss the lattice structure. As previously mentioned, the uniform limit of the DFS based on the SCL of ^{4}He cluster has a cubic Fermi surface while that of the DFS based on the SCL of ^{16}O cluster has an uneven Fermi surface given by Eq. (10). The energy of the uniform limit of the ^{16}O-cluster-like DFS is slightly lower than that of ^{4}He-cluster-like one. Since the lattice structure is reflected in the Fermi surface, we need to systematically investigate DFSs due to ^{4}He and ^{16}O clustering in the Bloch description including the transition of lattice structure.

TABLE II. Critical densities of DFSs due to ^{4}He, ^{16}O, and ^{10}He clustering.

^{4}He:0.22_{ρ_0}	^{16}O:0.32_{ρ_0}	^{10}He:0.22_{ρ_0}

D. Dependence of DFSs on effective forces

Finally, we state the dependence of DFSs on effective nuclear forces. Various kinds of effective nuclear forces have been proposed to satisfy the saturation property of nuclear matter [15,17–21]; furthermore, the shell-model-like and clusterlike aspects in finite nuclei are extensively studied using those forces [21–24]. In the Bloch description for nuclear

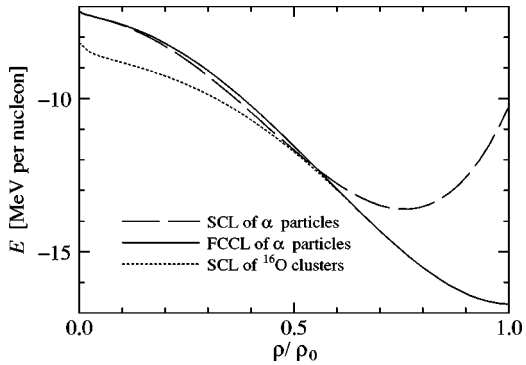

FIG. 7. Density dependence of energies per nucleon of the SCL (dashed line) and the FCCL (solid line) of α particles and the SCL of ^{16}O (dotted line). The density of matter is normalized by the saturation density of FCCL of α particles, $\rho_0=0.172$ fm^{-3}.

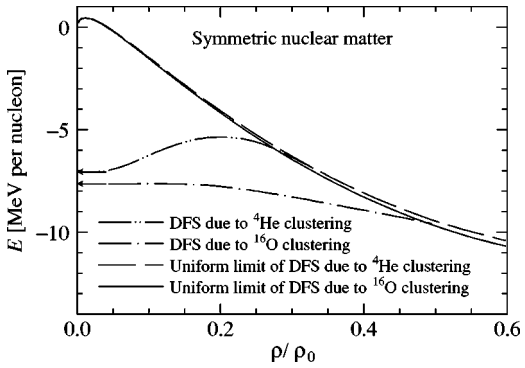

FIG. 8. Energy curves of DFSs due to α and ^{16}O clustering in the symmetric nuclear matter by the use of the BB (B_4) force. The density of matter is normalized by the saturation density of the uniform matter with the Fermi sphere, $\rho_0=0.206$ fm^{-3}. The presentation of the curves is similar to that in Fig. 4.

matter, the uniform limit of DFSs, $a/b\leqslant 1$, corresponds to a shell-model-like state in finite nuclei, while a DFS with $a/b>1$ corresponds to a clustering excited state.

We calculated the energies of DFSs due to ^{4}He and ^{16}O clustering by using the Brink-Boeker (BB) force [17] instead of the MV1 force. Figure 8 displays the energy behaviors of DFSs due to ^{4}He and ^{16}O clustering with respect to the density of matter in the case of B_4 parametrization of the BB force. Energy behaviors of DFSs are qualitatively similar both in the cases of MV1 and BB forces. However, the critical densities calculated by using the BB force are higher than those calculated by using the MV1 force. Using several parametrizations of MV1 and BB forces, the critical densities of the DFS due to ^{4}He clustering are listed in Table III in which the characteristics of the ^{4}He nucleus and the uniform symmetric nuclear matter with the Fermi sphere are also listed.

As clearly shown in Table III, the BB force tends to cause DFSs due to clustering more easily in low-density regions compared with the MV1 force at all parametrizations. This tendency is originated in the character of an effective force. To reproduce the saturation property of nuclear matter, the BB force possesses the anomalous Majorana parameter while the MV force possesses the δ-type three-body interaction. It is suggested that it may be easy for clustering aspects to appear as excited states in finite nuclei by the use of the BB force. Furthermore, by comparing the four kinds of parametrizations in the BB force, we can find that the tendency to form α cluster in medium is supposedly related to nuclear incompressibility. Thus, the Bloch description serves as a guide to study finite nuclei, and the manner in which clustering degrees of freedom respond in medium depending on what kind of an effective force is used.

IV. SUMMARY AND DISCUSSIONS

We have discussed DFSs of nuclear matter due to clustering below the saturation density. We assumed that clusters are formed in nuclear matter below the saturation density and that they make up a SCL. We described DFSs due to clustering by the Slater determinant where single-particle states of nucleons are represented by the Bloch function. The Bloch description has the advantage of smoothly representing DFSs from an aggregate of isolated clusters in extremely low-density regions in one limit and the uniform matter in relatively high-density regions in the other limit.

We treated DFSs due to ^{4}He and ^{16}O clustering in the symmetric nuclear matter and ^{10}He clustering in asymmetric nuclear matter with $Y_p=0.2$ by the tight-binding approximation including 0s and 0p orbits. We found that all DFSs have critical densities below which they are energetically favorable compared with the uniform state. In symmetric nuclear matter, the ^{16}O clustering gains energy for the system compared with ^{4}He clustering in any density region.

This feature remains after subtracting the spurious energy of each constituent cluster originating in its c.m. motion, which is approximately estimated on the basis of the kinetic energy of the s-wave Bloch function with $k=0$. The subtraction does not affect the critical density because the s-wave Bloch function is almost identical to the plane-wave function near the critical density. In a similar manner, the Coulomb energy is also not expected to affect the critical density under the assumption of a uniform background of electrons. This is because the uniform distribution of electrons cancels out the distribution of protons, which becomes almost uniform near the critical density.

TABLE III. The critical densities of the DFS due to ^{4}He clustering, which are normalized by the theoretical saturation density ρ_0, and characteristics of the ^{4}He nucleus, and uniform symmetric nuclear matter with the Fermi sphere by using several versions of MV1 and BB forces.

	DFS of ^{4}He		^{4}He		Uniform symmetric nuclear matter		
	ρ_{cr}/ρ_0	E(MeV)	R_{rms}(fm)	K(MeV)	E(MeV)	ρ_0 (fm^{-3})	K(MeV)
BB case B_1	0.41	−7.05	1.49	79	−15.69	0.205	183
BB case B_2	0.35	−7.06	1.49	90	−15.75	0.206	203
BB case B_3	0.33	−7.07	1.49	102	−15.80	0.206	225
BB case B_4	0.33	−7.06	1.49	113	−15.75	0.206	249
MV1 case 1	0.25	−7.23	1.64	99	−21.01	0.218	296
MV1 case 2	0.26	−7.43	1.63	101	−21.61	0.222	307
MV1 case 3	0.22	−7.19	1.61	97	−23.51	0.261	324

We have not discussed the DFS due to ^{10}He clustering in asymmetric nuclear matter, because the introduction of only the orthogonal *p*-wave Bloch function is not sufficient to describe ^{10}He clustering. The phenomena of halo and skin have been observed in the neutron-rich region. In order to treat the core and valence neutrons independently, we have to introduce the *s*- and *p*-wave Bloch functions with different width parameters or higher nodal orbital Bloch functions. This is one of the future subjects to broaden our study of the clustering phenomena in neutron-rich nuclear matter.

We also investigated the dependence of energy profiles of DFSs due to clustering on effective nuclear forces using two kinds of effective forces, namely, the MV1 and BB forces. We recognized that the critical densities depended on the kind of effective nuclear force used, although the qualitative behavior did not. The BB force tends to cause density fluctuation more easily in low-density regions compared with the MV1 force. It is suggested that it may be easy for clustering aspects to appear as excited states in finite nuclei using the BB force. The uniform limit, $a/b \simeq 1$, of the Bloch description corresponds to the shell-model-like ground state in finite nuclei, while a DFS with $a/b > 1$ corresponds to a clustering excited state. Thus, the Bloch description provides beneficial information for studies on finite nuclei on the basis of how clustering degrees of freedom respond in medium depending on what kind of effective force is used.

However, the present study cannot conclude that the DFS due to ^{16}O clustering is always energetically favorable as compared with the DFS due to ^{4}He clustering because we only considered DFSs with a SCL of clusters. Within the classical treatment, we pointed out that there exists the possibility that the SCL of ^{16}O clusters transits to the FCCL of α clusters near the critical density. In a similar manner, the crystalline structure of ^{56}Fe is certainly realized in extremely low-density regions such as the inner crust of neutron stars; however, it is also obscure near the critical density at which a DFS starts to develop. Besides the crystalline structure of nuclei, there have been recent theoretical investigations on the possibility of α cluster condensation in low-density nuclear matter [7,8]. If phase transition between the crystalline structures of nuclei and α condensation occur, constituent nuclei need to be excited to an α-gas state near the α-breakup threshold [24–26] owing to interference among nuclei at different lattice sites.

Therefore, our future task will aim to investigate the transition between DFSs due to α and ^{16}O clustering using the Bloch description in order to understand the clustering phenomena in nuclear matter. In the transition region between the SCL of ^{16}O nuclei and the FCCL of α clusters, constituent ^{16}O nuclei are excited to α-clustering states, which is capable of being a door-way state between the normal phase and α condensation in nuclear matter. Such an extension, where clusters are distributed within a unit cell, will lead to a microscopic study on the structure of the inner crust of neutron stars with zero temperature and supernova matter with finite temperature.

ACKNOWLEDGMENTS

One of the authors (H.T.) wishes to acknowledge the support provided by the Shinshu University.

[1] A. W. Overhauser, Phys. Rev. Lett. **4**, 415 (1967).
[2] Y. Fujiwara, H. Horiuchi, K. Ikeda, M. Kamimura, K. Kato, Y. Suzuki, and E. Uegaki, Suppl. Prog. Theor. Phys. **68**, 29 (1980).
[3] Y. Akaishi and H. Bandō, Prog. Theor. Phys. **41**, 1594 (1969).
[4] D. M. Brink and J. J. Castro, Nucl. Phys. **A216**, 109 (1973).
[5] A. Tohsaki, Prog. Theor. Phys. **81**, 370 (1989); **88**, 1119 (1992); **90**, 871 (1993).
[6] A. Tohsaki, Phys. Rev. Lett. **76**, 3518 (1996).
[7] G. Röpke, A. Schnell, and P. Schuck, Phys. Rev. Lett. **80**, 3177 (1998).
[8] M. Beyer, S. A. Sofianos, C. Kuhrts, G. Röpke, and P. Schuck, Phys. Lett. B **488**, 247 (2000).
[9] D. G. Ravenhall, C. J. Pethick, and J. R. Wilson, Phys. Rev. Lett. **50**, 2066 (1983).
[10] M. Hashimoto, H. Seki, and M. Yamada, Prog. Theor. Phys. **71**, 320 (1984).
[11] G. Peilert, J. Randrup, H. Stöcker, and W. Greiner, Phys. Lett. B **260** 271 (1991).
[12] T. Maruyama, K. Niita, K. Oyamatsu, T. Maruyama, S. Chiba, and A. Iwamoto, Phys. Rev. C **57**, 655 (1998).
[13] G. Watanabe, K. Sato, K. Yasuoka, and T. Ebisuzaki, Phys. Rev. C **66**, 012801(R) (2002).
[14] A. E. Pozamantir and A. W. Overhauser, Phys. Rev. C **64**, 014303 (2001).
[15] T. Ando, K. Ikeda, and A. Tohsaki- suzuki, Prog. Theor. Phys. **64**, 1608 (1980).
[16] H. Takemoto and A. Tohsaki, Prog. Theor. Phys. **111**, 213 (2004).
[17] D. M. Brink and E. Boeker, Nucl. Phys. **A91**, 1 (1967).
[18] M. Beiner, H. Flocard, Nguyen van giai, and P. Quentin, Nucl. Phys. **A238**, 29 (1975).
[19] J. Decharge and D. Gogny, Phys. Rev. C **21**, 1568 (1980).
[20] A. Tohsaki, Phys. Rev. C **49**, 1814 (1994).
[21] A. E. Pozamantir and A. W. Overhauser, Phys. Rev. C **64**, 014302 (2001).
[22] Y. Kanada-En'yo and H. Horiuchi, Phys. Rev. C **66**, 024305 (2002).
[23] M. Kimura, Y. Sugawa, and H. Horiuchi, Prog. Theor. Phys. **106**, 1153 (2001).
[24] A. Tohsaki, H. Horiuchi, P. Schuck, and G. Röpke, Phys. Rev. Lett. **87**, 192501 (2001).
[25] Y. Funaki, H. Horiuchi, A. Tohsaki, P. Schuck, and G. Röpke, Prog. Theor. Phys. **108**, 297 (2002).
[26] Y. Funaki, A. Tohsaki, H. Horiuchi, P. Schuck, and G. Röpke, Phys. Rev. C **67**, 051306(R) (2003).